WILLIAM & MARY
CHARTERED 1693

W&M ScholarWorks

Arts & Sciences Articles

Arts and Sciences

2015

Polarization Transfer in Wide-Angle Compton Scattering and Single-Pion Photoproduction from the Proton

C. Fanelli

G. Salme

E. Cisbani

A. Kelleher
College of William and Mary

M. Meziane
College of William and Mary

See next page for additional authors

Follow this and additional works at: https://scholarworks.wm.edu/aspubs

Recommended Citation

Fanelli, C., Cisbani, E., Hamilton, D. J., Salmé, G., Wojtsekhowski, B., Ahmidouch, A., ... & Brash, E. J. (2015). Polarization transfer in wide-angle Compton scattering and single-pion photoproduction from the proton. Physical review letters, 115(15), 152001.

Authors

C. Fanelli, G. Salme, E. Cisbani, A. Kelleher, M. Meziane, L. Pentchev, and C. F. Perdrisat

Polarization Transfer in Wide-Angle Compton Scattering and Single-Pion Photoproduction from the Proton

C. Fanelli,[1,2] E. Cisbani,[2] D. J. Hamilton,[3] G. Salmé,[1] B. Wojtsekhowski,[4,*] A. Ahmidouch,[5] J. R. M. Annand,[3]
H. Baghdasaryan,[6] J. Beaufait,[4] P. Bosted,[4] E. J. Brash,[7,4] C. Butuceanu,[8] P. Carter,[7] E. Christy,[9] E. Chudakov,[4]
S. Danagoulian,[5] D. Day,[6] P. Degtyarenko,[4] R. Ent,[4] H. Fenker,[4] M. Fowler,[4] E. Frlez,[6] D. Gaskell,[4] R. Gilman,[4,10]
T. Horn,[4] G. M. Huber,[8] C. W. de Jager,[4,6] E. Jensen,[7] M. K. Jones,[4] A. Kelleher,[11] C. Keppel,[9] M. Khandaker,[12] M. Kohl,[9]
G. Kumbartzki,[10] S. Lassiter,[4] Y. Li,[9] R. Lindgren,[6] H. Lovelace,[12] W. Luo,[13] D. Mack,[4] V. Mamyan,[6] D. J. Margaziotis,[14]
P. Markowitz,[15] J. Maxwell,[6] G. Mbianda,[16] D. Meekins,[4] M. Meziane,[11] J. Miller,[17] A. Mkrtchyan,[18] H. Mkrtchyan,[18]
J. Mulholland,[6] V. Nelyubin,[6] L. Pentchev,[11] C. F. Perdrisat,[11] E. Piasetzky,[19] Y. Prok,[7] A. J. R. Puckett,[20]
V. Punjabi,[12] M. Shabestari,[6] A. Shahinyan,[18] K. Slifer,[6] G. Smith,[4] P. Solvignon,[21] R. Subedi,[6]
F. R. Wesselmann,[12] S. Wood,[4] Z. Ye,[9] and X. Zheng[6]

[1]*Dipartimento di Fisica, Università La Sapienza, Rome, Italy
and INFN, Sezione di Roma, 00185 Rome, Italy*
[2]*INFN, Sezione di Roma, gruppo Sanità and Istituto Superiore di Sanità, 00161 Rome, Italy*
[3]*University of Glasgow, Glasgow G12 8QQ, Scotland, United Kingdom*
[4]*Thomas Jefferson National Accelerator Facility, Newport News, Virginia 23606, USA*
[5]*North Carolina A&T State University, Greensboro, North Carolina 27411, USA*
[6]*University of Virginia, Charlottesville, Virginia 22904, USA*
[7]*Christopher Newport University, Newport News, Virginia 23606, USA*
[8]*University of Regina, Regina, Saskatchewan S4S OA2, Canada*
[9]*Hampton University, Hampton, Virginia 23668, USA*
[10]*Rutgers, The State University of New Jersey, Piscataway, New Jersey 08855, USA*
[11]*College of William and Mary, Williamsburg, Virginia 23187, USA*
[12]*Norfolk State University, Norfolk, Virginia 23504, USA*
[13]*Lanzhou University, Lanzhou 730000, Gansu, People's Republic of China*
[14]*California State University Los Angeles, Los Angeles, California 90032, USA*
[15]*Florida International University, Miami, Florida 33199, USA*
[16]*University of Witwatersrand, Johannesburg, South Africa*
[17]*University of Maryland, College Park, Maryland 20742, USA*
[18]*Yerevan Physics Institute, Yerevan 375036, Armenia*
[19]*University of Tel Aviv, Tel Aviv 6997801, Israel*
[20]*Massachusetts Institute of Technology, Cambridge, Massachusetts 02139, USA*
[21]*Argonne National Laboratory, Argonne, Illinois 60439, USA*

Wide-angle exclusive Compton scattering and single-pion photoproduction from the proton have been investigated via measurement of the polarization transfer from a circularly polarized photon beam to the recoil proton. The wide-angle Compton scattering polarization transfer was analyzed at an incident photon energy of 3.7 GeV at a proton scattering angle of $\theta^p_{\mathrm{cm}} = 70°$. The longitudinal transfer K_{LL}, measured to be $0.645 \pm 0.059 \pm 0.048$, where the first error is statistical and the second is systematic, has the same sign as predicted for the reaction mechanism in which the photon interacts with a single quark carrying the spin of the proton. However, the observed value is ~3 times larger than predicted by the generalized-parton-distribution-based calculations, which indicates a significant unknown contribution to the scattering amplitude.

Understanding the structure of hadrons in terms of QCD is one of the fundamental goals of modern nuclear physics. The formalism of generalized parton distributions (GPDs), developed about 20 years ago, for the first time linked hadron structure information accessible through inclusive reactions such as deep inelastic scattering to information from exclusive reactions. These GPDs, while not directly measurable in experiments, provide a unified description of key

electromagnetic reactions on the nucleon [1]. Whereas deep inelastic scattering allows investigation of the longitudinal structure of the nucleon, exclusive reactions such as elastic electron and photon scattering access its transverse structure. Taken together they allow determination of a complete image of the nucleon and its complex substructure [2].

Wide-angle Compton scattering (WACS) from the nucleon with large values of s, $-t$, and $-u$ compared with

Λ^2_{QCD} is a hard exclusive process that provides access to information about nucleon structure that is complementary to high Q^2 elastic form factors and deeply virtual Compton scattering. The common feature of these reactions is a large energy scale, leading to factorization of the scattering amplitude into a hard perturbative kernel and a factor described by soft nonperturbative wave functions.

Various theoretical approaches have been applied to WACS in the hard-scattering regime, and these can be distinguished by the number of active quarks participating in the hard subprocess, or equivalently, by the mechanism for sharing the transferred momentum among the constituents. Two extreme pictures have been proposed. In the perturbative QCD (pQCD) approach, three active quarks share the transferred momentum by the exchange of two hard gluons [3,4]. In the handbag approach, which has in recent years become a staple in the interpretation of data from hard exclusive reactions, only one quark, whose wave function has sufficient high-momentum components for the quark to absorb and reemit the photon [5–7], is assumed to be active. In any given kinematic regime both mechanisms will contribute, in principle, to the cross section. It is generally believed that at sufficiently high energies the pQCD mechanism dominates. However, in the currently accessible experimental domain of s and t, the nature of the reaction mechanism is not fully understood.

Three other theoretical advances based on leading-quark dominance in WACS have been proposed in recent years. The constituent quark model (CQM) with a handbag diagram has proven successful in describing the WACS process [8], as have calculations performed in an extended Regge model [9]. More recently, the soft-collinear effective theory (SCET) was developed for elastic electron-proton scattering at high-momentum transfer [10]. The QCD factorization approach formulated in the framework of SCET allows for the development of a description of the soft-spectator scattering contribution to the overall amplitude. The two-photon exchange contributions to elastic electron-proton scattering were shown to factorize by the introduction of a single, universal SCET form factor which defines the dominant soft-spectator amplitudes. As it is argued in Ref. [10], the same form factor also arises naturally in WACS, and the most promising route for understanding this soft spectator contribution in hard exclusive reactions at JLab energies is the study of WACS.

One of the main predictions of the pQCD mechanism for WACS is the constituent scaling rule [11], whereby $d\sigma/dt$ scales as s^{-6} at fixed θ^p_{cm}. The pioneering experiment at Cornell [12] was approximately consistent with constituent scaling, albeit with modest statistical precision. However, the high-precision data from JLab gave a scaling power of $s^{-7.5\pm0.2}$ [13]. The calculations from both the GPD-based handbag approach and the SCET framework have reproduced the JLab cross section data very well. Crucially, the extracted values of the SCET form factor do not show any

significant dependence on the value of s as required by factorization.

The longitudinal and sideways polarization transfer observables, K_{LL} and K_{LS}, respectively, are defined by

$$K_{\text{LL}} \equiv \frac{d\sigma(+,\rightarrow) - d\sigma(-,\rightarrow)}{d\sigma(+,\rightarrow) + d\sigma(-,\rightarrow)},$$

$$K_{\text{LS}} \equiv \frac{d\sigma(+,\uparrow) - d\sigma(-,\uparrow)}{d\sigma(+,\uparrow) + d\sigma(-,\uparrow)},$$

where the first sign refers to the incident photon helicity and the arrow to the recoil proton longitudinal ($\rightarrow$) or sideways ($\uparrow$) polarization. The polarization transfer observables were previously measured at JLab for Compton scattering at $s = 6.9$ and $t = -4.1$ GeV^2 in experiment E99-114 [14], whose concept is mainly repeated here at different kinematics. It was found that the longitudinal component of the polarization transfer at the E99-114 kinematic point is large and positive, in agreement with the handbag GPD and SCET predictions in spite of a relatively low value of $u = -1.0$ GeV^2 and in unambiguous disagreement with the pQCD predictions.

The measurement reported in this Letter (JLab experiment E07-002) was carried out in Hall C at Jefferson Lab, with the purpose of providing values of K_{LL} and K_{LS} when all the Mandelstam variables are larger than Λ^2_{QCD}. The layout of the experiment is shown schematically in Fig. 1. A longitudinally polarized, 100% duty-factor electron beam with current up to 40 μA and energy of 4.11 GeV was incident on a copper radiator of 1.3 mm thickness placed on the beam line. The mixed beam of electrons and bremsstrahlung photons was incident on a 15 cm liquid H$_2$ target, located just downstream from the radiator, with a photon flux of up to 10^{13} equivalent quanta/s. For incident photons at an average weighted energy of 3.7 GeV, the scattered photons were detected at a scattering angle of 25.7° in the BigCal calorimeter, which is composed of 1744 lead-glass bars subtending a solid angle of 34 msr with an angular
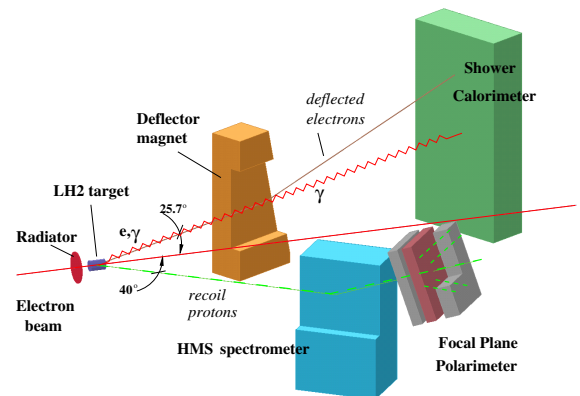

FIG. 1 (color online). Schematic layout of the E07-002 experiment.

resolution of 1.8 mrad and relative energy resolution of 12%. The associated recoil proton was detected in the Hall C High Momentum Spectrometer (HMS) at the corresponding central angle of 40° and central momentum of 1.85 GeV. The proton was detected within a solid angle of 5 msr and momentum acceptance of ±9%. The trigger was formed from a coincidence between a signal from scintillator counters in the HMS and a signal above a 500 MeV threshold in the calorimeter. A magnet between the target and the calorimeter, as shown in Fig. 1, with $\int \vec{B} \times \vec{dl} =$ 1.2 Tm deflected the elastically scattered electrons vertically by ~50 cm relative to undeflected WACS photons. Events with a radiative photon kinematically indistinguishable from WACS constitute an irreducible background.

Data have been collected with the radiator present and removed, and with different field settings of the deflection magnet. About 7.4 C of beam charge was accumulated for WACS production runs. The electron beam longitudinal polarization was found to be $75.0 \pm 1.1\%$ using a Møller polarimeter. During data taking, the beam polarization was flipped at a 30 Hz rate. The bremsstrahlung photon has 99% of the initial electron polarization over the energy range of current analysis.

Potential WACS events are selected based on the kinematic correlation between the scattered photon and the recoil proton. The known optical properties of the HMS are used to reconstruct the momentum, direction, and reaction vertex of the recoil proton, from which the reconstructed incident photon (electron) energy (assuming a γp and ep final state), E_{inc}, was determined. The δx and δy, the difference in x and y coordinates between the expected and measured locations of the scattered photon at the entrance of the calorimeter, were calculated. The distributions of events in the $(\delta x : \delta y)$ and $(E_{\text{inc}} : \delta y)$ planes are shown in Figs. 2 and 3, respectively.

The WACS events $p(\gamma, \gamma' p)$, which are concentrated in the peak at $\delta x, \delta y \sim 0$ cm, lie on top of a continuum background mainly related to the $p(\gamma, \pi^0 p)$ reaction, for which one of the photons is detected from the subsequent decay $\pi^0 \to \gamma\gamma$. An additional background is due to electrons and radiative photons from elastic ep scattering.

The recoil proton polarization was measured by the focal plane polarimeter (FPP) located in the HMS. The FPP determines the two polarization components normal to the momentum of the proton by measuring the azimuthal asymmetries in the angular distribution after secondary scattering of the proton from an analyzer for positive and negative electron beam-helicity states. Two 60 cm (53 g/cm^2) thick blocks of CH$_2$ analyzers were used in the experiment. Two drift chambers at the focal plane, and a pair of large-acceptance drift chambers placed after each analyzer, tracked the protons before, between, and after the analyzer blocks, effectively producing two independent polarimeters with a combined figure of merit (a product of efficiency and analyzing power in square) of 7×10^{-3}.
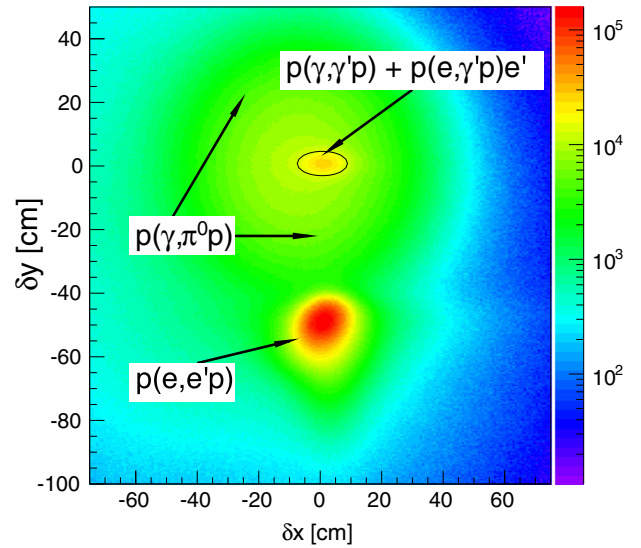

FIG. 2 (color online). Two-dimensional distribution of events in $(\delta x : \delta y)$. The WACS events $p(\gamma, \gamma' p)$ and the irreducible Bethe-Heitler background $p(e, \gamma' p)e'$ form the peak at $\delta x, \delta y \sim 0$ cm, which is selected by an elliptical cut $(\delta x/8)^2 + (\delta y/4)^2 < 1$. This region also contains the photopion events $p(\gamma, \pi^0 p)$—the underlying continuum. The ep elastic events are centered at $\delta x \sim 0$, $\delta y \sim -50$ cm.
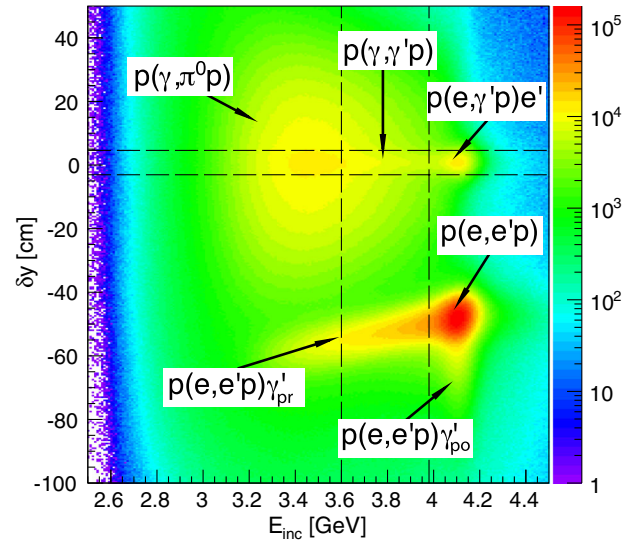

FIG. 3 (color online). Two-dimensional distribution of events in $(E_{\text{inc}} : \delta y)$. WACS $p(\gamma, \gamma' p)$ events are concentrated around $\delta y \sim 0$ cm, selected through an elliptical cut in $(\delta x : \delta y)$, and reconstructed $E_{\text{inc}} \in [3.60, 3.98]$ GeV. The $p(e, \gamma' p)e'$ events, with a high-energy postscattering radiative photon, are at $E_{\text{inc}} = 4.1$ GeV. Photopion $p(\gamma, \pi^0 p)$ events are mainly located at $\delta y \sim 0$ cm and $E_{\text{inc}} < 3.6$ GeV. At $\delta y = -50$ cm and $E_{\text{inc}} = 4.1$ GeV, elastic $p(e, e' p)$ events form a peak, with a vertical tail in δy of $p(e, e' p)\gamma'_{\text{po}}$ with a postscattering radiative photon, and an oblique tail of $p(e, e' p)\gamma'_{\text{pr}}$ with a prescattering radiative photon.

For each analyzer, the angular distribution of the scattered protons is given by

$$N(\vartheta, \varphi) = N_0(\vartheta)\{1 + [A_y(\vartheta)P_t^{\mathrm{FPP}} + \alpha]\sin\varphi$$
$$- [A_y(\vartheta)P_n^{\mathrm{FPP}} + \beta]\cos\varphi\},$$

where N_0 is the number of protons that scatter in the polarimeter, ϑ and φ are the polar and azimuthal scattering angles, P_n^{FPP} or P_t^{FPP} is the helicity-dependent component of the proton polarization at the FPP, A_y is the FPP analyzing power, and α and β are helicity-independent terms including instrumental asymmetries. Such a distribution was measured for the two states of the electron beam helicity. The difference between these two distributions, $N^+/N_0^+ - N^-/N_0^-$, cancels the instrumental asymmetries to first order and gives access to the helicity-dependent transferred polarization. Performing a Fourier analysis of the beam-helicity difference of $N(\vartheta, \varphi)$ allows extraction of the products of the proton polarization components and A_y, shown in Fig. 4.

Determination of $A_y(\vartheta)$ for each of the analyzers was performed by measuring the longitudinal polarization of the recoil proton from $\vec{e}p$ elastic scattering at approximately the same proton momentum. This analysis also yields the ratio of the proton elastic form factors, which was found to be $\mu_p G_E^p/G_M^p = 0.744 \pm 0.031$ at $Q^2 = 2.25\ \mathrm{GeV}^2$, in excellent agreement with a fit to known measurements [15].

Polarization components at the FPP were related to their counterparts at the target by calculating the proton spin precession in the HMS. This was done by using a COSY model [16] of the HMS optics to obtain a spin transport matrix for each proton track. The elements of this matrix
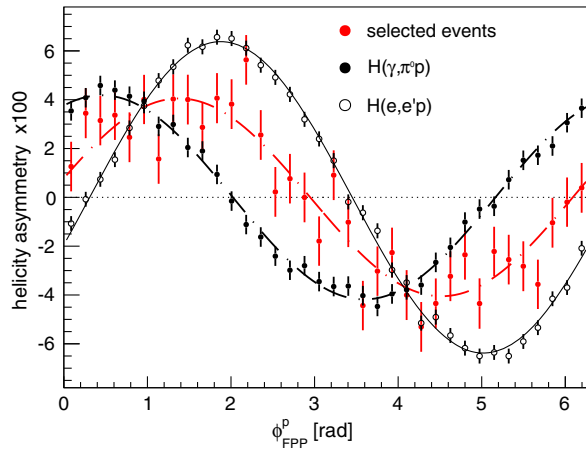

FIG. 4 (color online). Azimuthal variation of the difference between beam-helicity correlated proton rates. The selected events (filled red circles) are identified with an elliptical cut; see Fig. 2. Also shown are the corresponding asymmetries for the main background events: the elastic ep (open white circles) and photopion (filled black circles).

are characterized by the average spin precession angle, which is approximately 100°. The proton spin vector was then transformed to the proton rest frame, with the longitudinal axis pointing in the direction of the recoil proton in the center-of-mass frame [6]. In that frame, the longitudinal and sideways components of the proton polarization normalized to the photon polarization are just the spin transfer parameters K_{LL} and K_{LS}, respectively.

The WACS events are selected from a small elliptical region at the origin of the $(\delta x : \delta y)$ plane, as shown in Fig. 2. For each spin component, the following deconvolution procedure has been used to extract the final WACS recoil polarization K_{WACS}:

$$K_{\mathrm{peak}} = [K_{\mathrm{ellipse}} - (1 - f_1)K_{\mathrm{pion}}]/f_1,$$
$$K_{\mathrm{WACS}} = [K_{\mathrm{peak}} - (1 - f_2)K_{ep\gamma}]/f_2,$$

where K_{ellipse}, K_{peak}, K_{pion}, and $K_{ep\gamma}$ are the polarizations related to (i) all of the events within the $(\delta x : \delta y)$ ellipse shown in Fig. 2, (ii) only the events in the peak above the continuum background, (iii) the pion photoproduction background events, and (iv) the Bethe-Heitler background events. The fractions for the ratio of event types are defined as $f_1 = N_{\mathrm{peak}}/N_{\mathrm{ellipse}}$ and $f_2 = N_{\mathrm{WACS}}/N_{\mathrm{peak}}$, respectively. The dominant background polarization, by itself an important physics result, K_{pion}, was measured by selecting events from regions of the $(\delta x : \delta y)$ plane in Fig. 2 that contain neither WACS nor ep ($ep\gamma$) events, corresponding to $\delta y > 10$ cm and $-35 < \delta y < -10$ cm. It was found that within the statistical precision of the measurements, K_{pion} was constant over broad regions of that plane. The polarization of the $ep\gamma$ background $K_{ep\gamma}$ was determined by selecting events in the deflected ep elastic peak region. It was determined that within the statistical precision, the polarization K_{ep} was consistent with $K_{ep\gamma}$. The results for the longitudinal and sideways components are $K_{ep\gamma,\mathrm{LL}} = 0.4513 \pm 0.0054$ and $K_{ep\gamma,\mathrm{LS}} = -0.1837 \pm 0.0054$. Systematic uncertainties arising from the methods used to determine the background polarization observables have been studied and included in the final results. The final source of background which needs to be taken into account arises as a result of the presence of accidental random events in the final sample ($< 4\%$ of the events).

Results obtained with the two polarimeters were statistically consistent and were combined to form a weighted mean. With the WACS region selected to obtain the best statistical accuracy on K_{WACS} and fits performed on the respective distributions, we find $f_1 = 0.405 \pm 0.004$. The determination of the fraction f_2 is a little more involved and requires analysis of calibration data taken without the copper radiator. By doing so, we measure the quantity $n_{ep\gamma} = N_{ep\gamma}/N_{ep}$ after having imposed an optimized cut on the incident energy to remove prevertex interactions, which can then be used to determine the fraction

TABLE I. The WACS and pion photoproduction polarization results. In this experiment the values of the Mandelstam variables are $s = 7.8$ (0.3) and $t = -2.1$ (0.1) GeV^2, which define $\theta_{cm}^p = 70$ (2)°. The values in parentheses are the acceptance ranges. For the WACS polarization the first uncertainty is statistical and the second is systematic. For the pion photoproduction polarization the combined uncertainty is shown. In E99-114 (Ref. [14]), $s = 6.9$ GeV^2 and $\theta_{cm}^p = 120°$.

Selection	K_{LL}	K_{LS}
Ellipse	0.180 ± 0.015	-0.233 ± 0.015
Peak	0.565 ± 0.038	-0.142 ± 0.038
WACS$_{this\,experiment}$	$0.645 \pm 0.059 \pm 0.048$	$-0.089 \pm 0.059 \pm 0.040$
WACS$_{E99-114}$	$0.678 \pm 0.083 \pm 0.04$	$0.114 \pm 0.078 \pm 0.04$
Pion$_{this\,experiment}$	-0.082 ± 0.007	-0.296 ± 0.007
Pion$_{E99-114}$	0.532 ± 0.006	0.480 ± 0.006

$f_2 = 1 - N_{ep\gamma}/N_{peak} = 1 - n_{ep\gamma} \times N_{ep}/N_{peak}$ for the production data. Following this method, we find $f_2 = 0.67 \pm 0.03$. As a consistency check, this fraction was determined using a second analysis method which involved reconstructing the incident energy spectrum for $ep\gamma$ events through a convolution of the theoretical bremsstrahlung spectrum from the radiator with the real spectrum of calibration events (without the radiator) for a scattered photon detected at $\delta y \sim 0$ cm. A third method consists of extracting the fraction from the difference between the value of the cross section measured in this experiment, which includes the irreducible $ep\gamma$ background, and the value of the WACS cross section obtained from the parametrization of the E99-114 results [13]. The results obtained for f_2 using these three methods were found to be consistent with each other.

The extracted polarization transfer observables for different event samples are given in Table I. A comparison between the E99-114 [14] and the present polarization measurement results for WACS and a single-pion photoproduction is also given in Table I. The large changes of K_{LL}, K_{LS} in pion production between the two data sets indicate a complicated nonasymptotic reaction mechanism. These results are in good agreement with previous measurements [17].

The final result for WACS K_{LL} is shown in Fig. 5 along with the predictions of the relevant calculations. In agreement with what was found in the previous JLab experiment [14], the K_{LL} result is inconsistent with predictions based on the pQCD theory [4] and hence suggests that even at this experiment's values of $s, -t, -u = 7.8, 2.1, 4.0$ GeV^2 we are still far from the asymptotic regime for the WACS process. Figure 5 shows the pQCD predictions for the two extreme choices of the distribution amplitudes, namely, the asymptotic and COZ [19], with the first, $\phi_1(x_1, x_2, x_3) = 120 x_1 x_2 x_3$, for asymptotically large energy scales, and the second having a peak in ϕ_1 at $x_{1,3} \approx 1/2$, $x_2 \approx 0$, to be constrained by the QCD sum-rules-based values of its lowest moments.
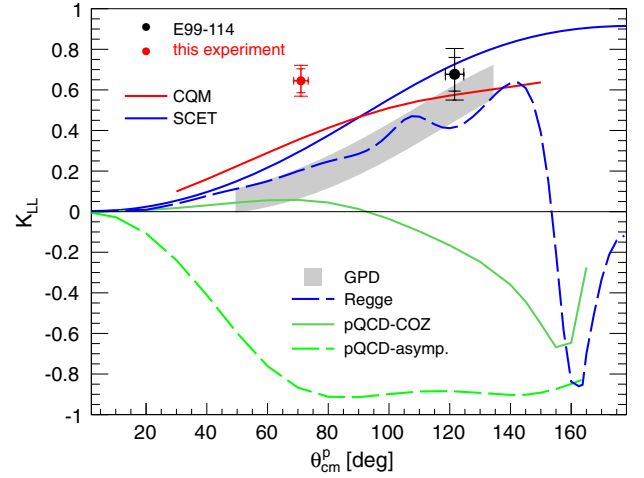

FIG. 5 (color online). The experimental result for K_{LL}. Also shown are the E99-114 value [14] and the calculations in different approaches: the pQCD [4] with the asymptotic and COZ distribution amplitudes [19], the extended Regge model [9], the GPD [7], shown as a gray band of uncertainty due to finite mass corrections [18], the CQM [8], and the SCET [10].

In conclusion, the polarization transfer observables K_{LL} and K_{LS} have been measured for proton Compton scattering at a new kinematic point at $s = 7.8$ GeV^2 and $\theta_{cm}^p = 70°$. The final results are $K_{LL} = 0.645 \pm 0.059 \pm 0.048$ and $K_{LS} = -0.089 \pm 0.059 \pm 0.040$, where the first uncertainty is statistical and the second is systematic. The K_{LS} result is in agreement within the experimental uncertainties with calculations for both the leading-quark and the pQCD approaches [4,7,8,10] and hence suggests that there is no strong evidence for proton helicity flip in this reaction. The value obtained for K_{LL} is, quite unexpectedly, larger than all the available theoretical predictions. Such a K_{LL} could be caused by noncollinear effects in exclusive reactions at currently accessible energies and parton correlations in the nucleon. In this respect, the K_{LL} increase may be related to significant roles observed in elastic electron-nucleon scattering of both quark orbital angular momentum and a u-d diquark correlation [20,21].

*Corresponding author.
bogdanw@jlab.org

[1] D. Müller, D. Robaschik, B. Geyer, F.-M. Dittes, and J. Hořejši, Fortschr. Phys. **42**, 101 (1994); X. D. Ji, Phys. Rev.

Lett. **78**, 610 (1997); A. V. Radyushkin, Phys. Lett. B **380**, 417 (1996).

[2] A. V. Belitsky and A. V. Radyushkin, Phys. Rep. **418**, 1 (2005).

[3] G. R. Farrar and H. Zhang, Phys. Rev. Lett. **65**, 1721 (1990); Phys. Rev. D **41**, 3348 (1990).

[4] A. S. Kronfeld and B. Nizic, Phys. Rev. D **44**, 3445 (1991); M. Vanderhaeghen, P. A. M. Guichon, and J. Van de Wiele, Nucl. Phys. **A622**, c144 (1997); T. Brooks and L. Dixon, Phys. Rev. D **62**, 114021 (2000).

[5] A. V. Radyushkin, Phys. Rev. D **58**, 114008 (1998).

[6] M. Diehl, T. Feldmann, R. Jakob, and P. Kroll, Eur. Phys. J. C **8**, 409 (1999).

[7] H. W. Huang, P. Kroll, and T. Morii, Eur. Phys. J. C **23**, 301 (2002); **31**, 279(E) (2003).

[8] G. A. Miller, Phys. Rev. C **69**, 052201(R) (2004).

[9] F. Cano and J. M. Laget, Phys. Lett. B **551**, 317 (2003).

[10] N. Kivel and M. Vanderhaeghen, J. High Energy Phys. 04 (2013) 29; Nucl. Phys. **B883**, 224 (2014); arXiv: 1504.00991.

[11] S. J. Brodsky and G. Farrar, Phys. Rev. Lett. **31**, 1153 (1973); V. A. Matveev, R. M. Muradyan, and A. V. Tavkheldize, Lett. Nuovo Cimento **7**, 719 (1973).

[12] M. A. Shupe *et al.*, Phys. Rev. D **19**, 1921 (1979).

[13] A. Danagoulian *et al.*, Phys. Rev. Lett. **98**, 152001 (2007).

[14] D. J. Hamilton *et al.*, Phys. Rev. Lett. **94**, 242001 (2005).

[15] A. J. R. Puckett *et al.*, Phys. Rev. C **85**, 045203 (2012); V. Punjabi *et al.*, Phys. Rev. C **71**, 055202 (2005); **71**, 069902 (2005).

[16] K. Makino and M. Berz, Nucl. Instrum. Methods Phys. Res., Sect. A **427**, 338 (1999).

[17] K. Wijesooriya *et al.*, Phys. Rev. C **66**, 034614 (2002); W. Luo *et al.*, Phys. Rev. Lett. **108**, 222004 (2012).

[18] M. Diehl, Th. Feldmann, H. W. Huang, and P. Kroll, Phys. Rev. D **67**, 037502 (2003).

[19] V. L. Chernyak, A. A. Oglobin, and A. R. Zhitnitsky, Z. Phys. C **42**, 569 (1989).

[20] M. Jones *et al.*, Phys. Rev. Lett. **84**, 1398 (2000); O. Gayou *et al.*, Phys. Rev. Lett. **88**, 092301 (2002); G. A. Miller, Phys. Rev. C **66**, 032201(R) (2002).

[21] G. D. Cates, C. W. de Jager, S. Riordan, and B. Wojtsekhowski, Phys. Rev. Lett. **106**, 252003 (2011); C. D. Roberts, M. S. Bhagwat, A. Höll, and S. V. Wright, Eur. Phys. J. Spec. Top. **140**, 53 (2007); I. C. Cloët, G. Eichmann, B. El-Bennich, T. Klähn, and C. D. Roberts, Few-Body Syst. **46**, 1 (2009).